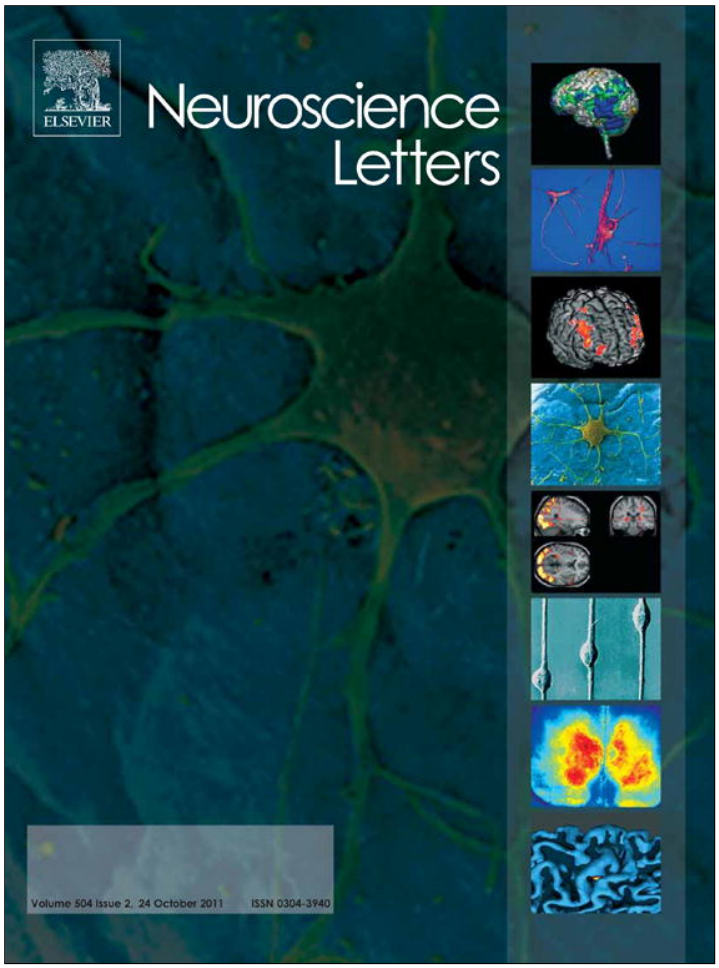

Neuroscience Letters 504 (2011) 115–120

Contents lists available at SciVerse ScienceDirect

Neuroscience Letters

journal homepage: www.elsevier.com/locate/neulet

# Recognition of stimulus-evoked neuronal optical response by identifying chaos levels of near-infrared spectroscopy time series

Xiao-Su Hu[a,1], Keum-Shik Hong[a,b,*], Shuzhi Sam Ge[a,c,d,2]

[a] Department of Cogno-Mechatronics Engineering, Pusan National University, 30 Jangjeon-dong, Gumjeong-gu, Busan 609-735, Republic of Korea
[b] School of Mechanical Engineering, Pusan National University, 30 Jangjeon-dong, Gumjeong-gu, Busan 609-735, Republic of Korea
[c] Department of Electrical & Computer Engineering, The National University of Singapore, Singapore 117576, Singapore
[d] The Robotics Institute, School of Computer Science and Engineering, University of Electronic Science and Technology of China, Chengdu 611813, China

ARTICLE INFO

*Article history:*
Received 2 July 2011
Received in revised form 10 August 2011
Accepted 9 September 2011

*Keywords:*
Brain signal
Neuronal optical response
Near-infrared spectroscopy (NIRS)
Chaotic characteristics

ABSTRACT

Near-infrared spectroscopy (NIRS) can detect two different kinds of signals from the human brain: the hemodynamic response (slow) and the neuronal response (fast). This paper explores a nonlinear aspect in the tactile-stimulus-evoked neuronal optical response over a NIRS time series (light intensity variation). The existence of the fast optical responses (FORs) over the time series recorded in stimulus sessions is confirmed by event-related averaging. The chaos levels of the NIRS time series recorded both in stimulus and in rest sessions are then identified according to the estimated largest Lyapunov exponent. The obtained results ascertain that stimulus-evoked neuronal optical responses can be detected in the somatosensory cortex using continuous-wave NIRS equipment. Further, the results strongly suggest that the chaos level can be used to recognize the FORs in NIRS time series and, thereby, the state of the pertinent brain activity.



Non-invasive brain-imaging technologies have vastly enhanced the ability to observe human brain functioning at the macroscopic level. A number of modalities of non-invasive brain activity imaging and measurement have been developed: One such modality, which includes electroencephalography (EEG) and magnetoencephalography (MEG), records neuronal-activity-related signals at the scalp (the electrophysiological response). These offer excellent temporal resolution on the order of milliseconds but limited spatial resolution. Another modality, which includes functional magnetic resonance imaging (fMRI), measures the oxygen level variation in the cerebral blood (the hemodynamic response), providing outstanding spatial resolution in millimeters but poor temporal resolution.

In recent years, a new brain-imaging technology reconciling spatial and temporal resolution, near-infrared spectroscopy (NIRS), has been utilized in investigations of stimulus/task-evoked brain functions of adult brains [2,13,19,20], infant brains [15], and neural diseases [25]. NIRS offers the advantages of low cost, insensitivity to motion artifacts, and potability. Furthermore, NIRS can measure two different kinds of optical signals from the human brain: hemodynamic (slow) response and neuronal (fast) response [19].

NIRS detects hemodynamic changes in brain blood in the following ways: near-infrared wavelengths in the 700–1000 nm range are irradiated onto the head; this light penetrating the scalp is either reflected or absorbed by the blood chromophores in the brain tissue [19]; the light intensity at a specific position is measured to detect the localized concentration changes of the blood chromophores, oxygenated hemoglobin and deoxygenated hemoglobin. NIRS can also detect stimulus/task-evoked localized neuron-optical-properties variation, which are faster optical responses compared to those prompted by hemodynamic changes. The NIRS-detected neuronal response is termed either a fast optical response (FOR) or an event-related optical signal (EROS). A neuron's FORs coincide with its electrophysiological responses [3]. These, normally occurring on the millisecond scale, are prompted by light-scattering-property changes associated with neuronal swelling and extracellular space changes due to ion currents crossing the neuronal membrane [8,9,19].

The FOR is very attractive in optical brain imaging due to its outstanding temporal resolution and good spatial resolution. Gratton and Fabiani [8] reported that the location of FORs detected by NIRS was consistent with fMRI detection and that the latency of the response was comparable to the EEG-measured visual evoked

* Corresponding author at: School of Mechanical Engineering, Pusan National University, 30 Jangjeon-dong, Gumjeong-gu, Busan 609-735, Republic of Korea.
Tel.: +82 10 8862 2454; fax: +82 51 514 0685.
*E-mail addresses:* x.hu@pusan.ac.kr (X.-S. Hu), kshong@pusan.ac.kr (K.-S. Hong), samge@nus.edu.sg (S.S. Ge).
[1] Tel.: +82 51 510 2973; fax: +82 51 514 0685.
[2] Tel.: +65 6516 6821; fax: +65 6779 1103.

0304-3940/$ – see front matter © 2011 Elsevier Ireland Ltd. All rights reserved.
doi:10.1016/j.neulet.2011.09.011

potential (VEP). Hence the FOR is very useful in studying neuronal vascular coupling, and can also aid cognitive studies that require both temporal and spatial resolution.

In the last decade, a number of investigations have been carried out on different aspects of FOR as detected in various human brain cortical areas by NIRS. Gratton et al. [6] discovered FORs in the visual cortex with frequency-domain NIRS equipment, and analyzed the ways in which heart-pulse noises in NIRS time series interfere with FOR detection in the brain. Later, they revealed the linear relationship between FORs and hemodynamic responses [12], and used a larger data set to investigate FORs' replicability, consistency, localization, and resolution [7]. Furthermore, they investigated FORs in other brain cortical areas including the somatosensory cortex [11] and the motor cortex [10]. Rinne et al. [21] reported two FOR components with different delays, 100 ms and 160 ms, in the auditory cortex. Steinbrink et al. [24] detected FORs evoked by median nerve stimulation in the parietal cortical region using continuous-wave NIRS equipment.

Meanwhile, some studies have reported less promising results: Steinbrink et al. [23], for instance, found that the FORs, detected in the visual cortex, were much smaller in magnitude than those found by the Gratton group. Franceschini and Boas [4] investigated the FORs evoked by finger tapping (motor cortex), tactile stimulation, and electrical median nerve stimulation (somatosensory cortex) in 10 healthy volunteers; they were able to detect FORs in 43% of the measurements during finger tapping, 60% of those during tactile stimulation, and 23% of those during electrical median nerve stimulation. Several research groups have utilized independent component analysis (ICA) to separate FOR signals and noises from raw NIRS time series, concluding that the ICA is a promising approach to detect fast neuronal signals [17,18].

Although there have been many computational analyses on obtaining FORs, no work has yet examined their nonlinear aspects. Barbour et al. [1] investigated the chaotic behavior of the vasculature in a large tissue structure. Moreover, Truong et al. [26] reported that some hemodynamic-response time series detected by NIRS are chaotic, and that the chaos level can be treated as an index to distinguish different brain states (task vs. rest). This study explores the chaotic characteristics of FOR time series. The FORs are small in magnitude compared to noises in NIRS time series (e.g. heart-pulse noise). We use the ICA to remove the non-relevant noises, after which an event-related averaging is employed to find the FORs over the NIRS time series. The estimation algorithm in [22] was then utilized to identify the chaos levels of the NIRS time series.

The data were acquired with a continuous-wave NIRS imaging system (DYNOT: DYnamic Near-infrared Optical Tomography; NIRx Medical Technologies, Brooklyn, NY) at a sampling rate of 41 Hz. The NIRS system emits laser light at different wavelengths (760 nm and 830 nm) from the source. Fig. 1(a) shows the channel distribution and measurement locations. The distance between adjacent optodes is 1 cm. The source-detector pairs are positioned above the somatosensory cortex (the C3 position, according to the international 10/20 system).

The DYNOT equipment employed in the current study incorporates optical fiber cables designed to support both emitting and receiving light [17]. This is based on the concept of "collocated" channel (i.e. the source and detector locations are the same: see the source 1-detector 1 pair in Fig. 1(b)), which is capable of capturing light reflected by tissues at a very superficial layer (<3 mm). The signal detected from this volume contains mainly noises. The optodes positioned at greater distances capture light propagating along a banana-shaped path that has successively greater maximum depths. In the current study, we took advantage of this optodes setting when applying the ICA to NIRS time series processing.

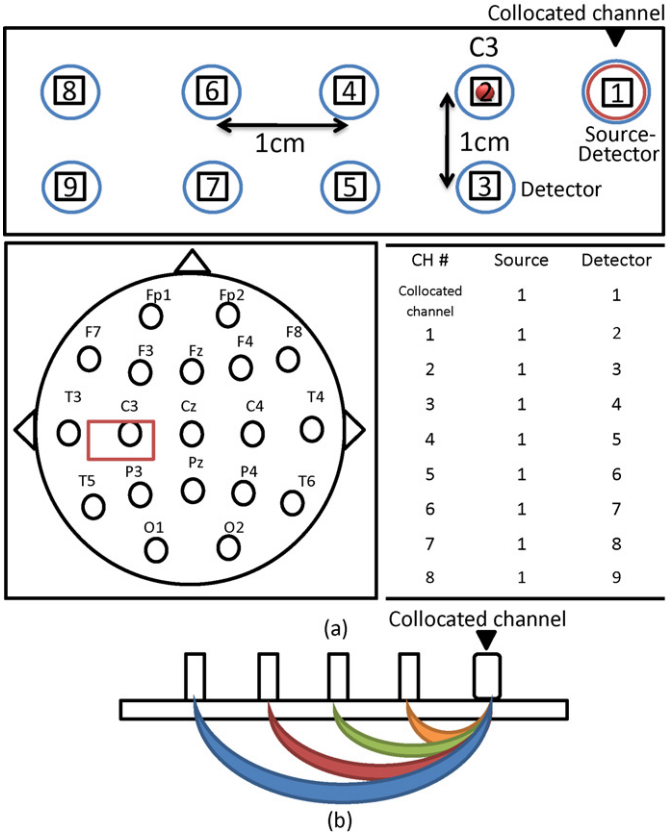


**Fig. 1.** Channel distribution and measurement location on the head.

Ten right-handed healthy volunteers (all males, aged 24–31 years) participated in this experiment. None of the participants had a history of any neurological disorder. All of the participants provided written informed consent. In the experiment, the subjects received 2 Hz tactile stimuli in their right hand. The experiment consisted of a 30 s preparation period, a 10 min stimulation period including alternating 30 s rest and tactile stimulus sessions (the rest and stimulus sessions were each repeated 10 times), and a 30 s after-exercise period. For control purpose, the tactile stimuli were also applied to the ipsilateral hand (left hand) of each subject following the same paradigm. Throughout the experimental period, optical data were recorded at a sampling rate of 41 Hz. To remove the hemodynamic response, very-low-frequency components, and physiological noises (e.g. Mayer wave, around 0.1 Hz, respiration noise, around 0.25 Hz, and heart pulse noise, around 1 Hz) from the optical signal, the data were high-pass filtered at >1 Hz. After their base-line correction, the data were subjected to ICA.

NIRS data usually has a huge number of temporal samplings (e.g. 11 min recording at 41 Hz sampling rate) but a relatively small number of channels (e.g. 9 channels). The ICA therefore is suitable for NIRS data processing, and indeed, it has been widely employed in task-related NIRS studies [17,18].

The rationale for using ICA in the current study was that the noises were statistically independent of, and therefore separate from, all of the other components, those representing neuronal activities of interest. ICA decomposes a signal into its statistically independent components that are linearly related to the original data [14]. In the current study, we used the ICA algorithm introduced in [14]. Let $M$ and $N$ denote the number of channels and that of data points, respectively (in this study, $M = 9$ and $N = 27{,}060$). Let $\boldsymbol{Y} \in R^{M \times N}$ and $\boldsymbol{S} \in R^{M \times N}$ be the matrices representing the data points observed and the independent components to be estimated, respectively. Then, the linear relationship between $\boldsymbol{Y}$ and $\boldsymbol{S}$ can

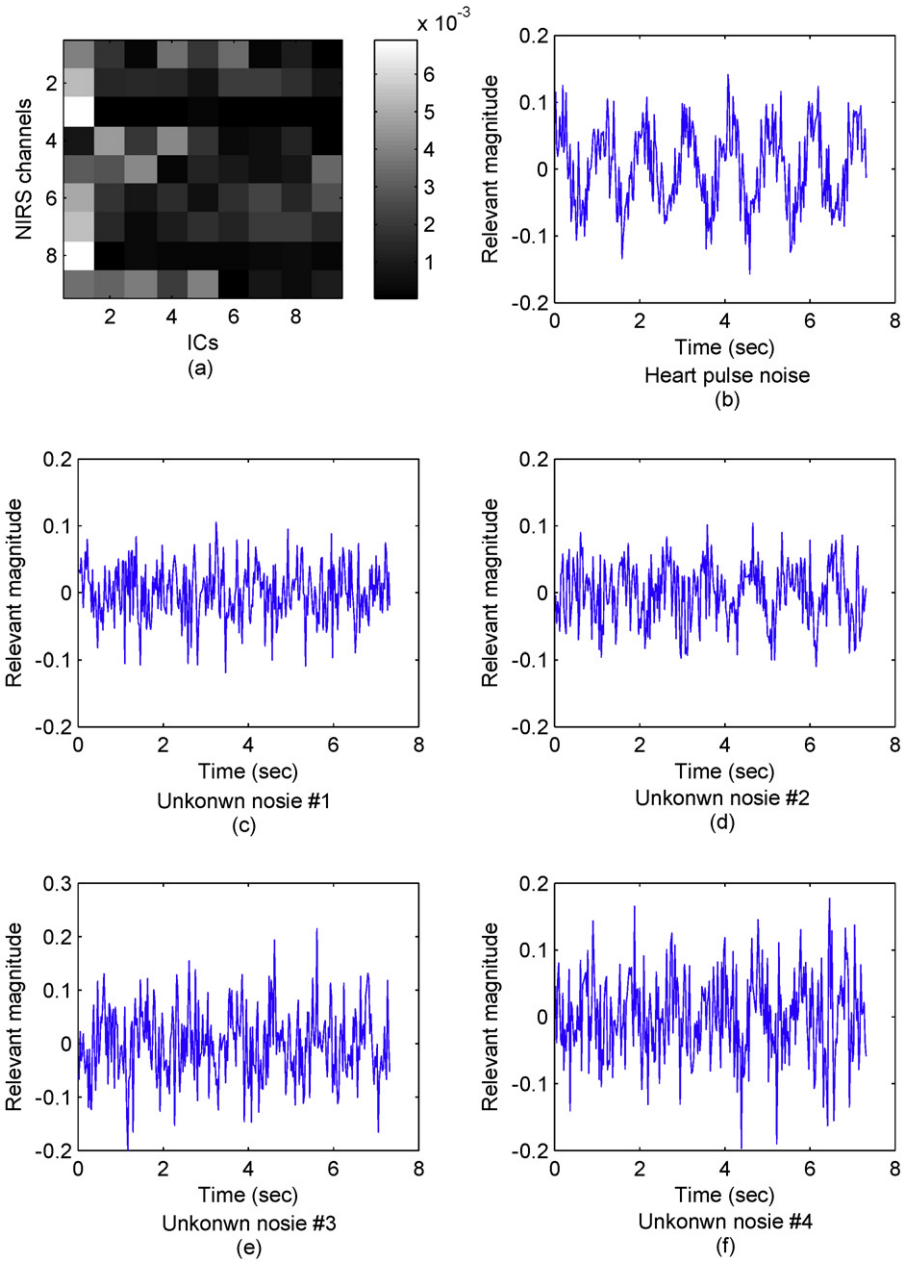


**Fig. 2.** ICA and noise separation (subject 1, wavelength 760 nm): (a) A representative transformation matrix $\boldsymbol{A}$. (b–f) Five representative independent noise components (heart pulse noise can be found in (b)).

be written in matrix form as $\boldsymbol{Y}=\boldsymbol{A}\cdot\boldsymbol{S}$, where $\boldsymbol{A}\in R^{M\times M}$ is the transformation matrix. The ICA tries to find the matrix $\boldsymbol{A}$ along with the component matrix $\boldsymbol{S}$, in which the components are statistically independent (non-Gaussian distribution) upon the observed data $\boldsymbol{Y}$.

The transformation matrix $\boldsymbol{A}$ represents the weight that individual independent components contribute to the measured signal. The independent components resulting in a high transformation weight contributing to the signal detected from a collocated channel are likely to represent noises in the raw data. These components therefore need to be removed from the component matrix $\boldsymbol{S}$, after which the modified component matrix, free of (separated) noises, is restored into the observed signal.

After pre-processing, the signal in each data channel was recalculated to its relative value ($\Delta I/I_0$), where $\Delta I$ referred to the concentration change at different sample points, and $I_0$ was the initial value of the data series. We segmented the data recorded in the stimulus sessions for each channel and each subject into stimulus-related 0–500 ms epochs after the onset of the tactile stimuli (both the contralateral and ipsilateral hand, the data in 1 s was segmented into two epochs due to the 2 Hz stimulus frequency). In one stimulus session (30 s), 60 stimulus-related epochs were totally generated. The data series recorded in the rest sessions were segmented following a similar pattern for the purpose of comparison. In one rest session (30 s), 60 rest-related epochs were totally generated.

The data series measured from each channel in both the stimulus-related and rest-related epochs were first averaged for each subject. The channel containing the FORs was statistically assessed using $t$-test ($p<0.05$) for every subject. The representative signals were then averaged across subjects giving a group level result, which was also assessed against the baseline using $t$-test

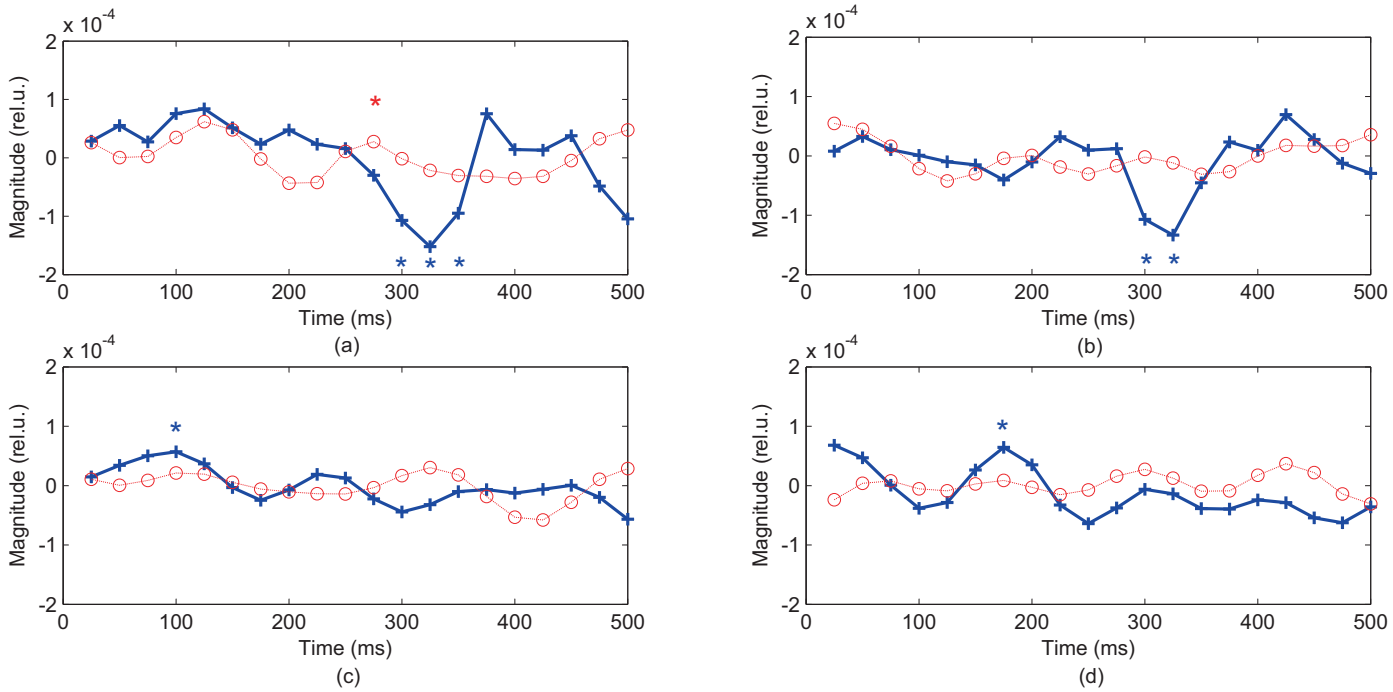


**Fig. 3.** The group level tactile-stimulus-evoked FORs (the blue line (+) depicts the averaged stimulus related epochs; the red line (○) shows the rest related epochs; the asterisk means a significant $t$-value ($p < 0.05$); $n$ indicates the subject number): (a) wavelength 760 nm ($n = 8$), (b) wavelength 830 nm ($n = 7$), (c) wavelength 760 nm under the control condition ($n = 8$), and (d) wavelength 830 nm under the control condition ($n = 7$). (For interpretation of the references to color in this figure legend, the reader is referred to the web version of the article.)

($p < 0.05$). Under the control condition, the averaged signal was derived based on the data measured from the same channel as in the previous stage. The group averaged responses were calculated separately for two wavelengths. If in a given subject no channel showed significant deviation, this subject (with specific wavelength) was excluded from the group averaging.

The presence of chaos in a dynamical system can be evaluated by estimating the largest Lyapunov exponent (LLE). The LLE is a quantity that characterizes the rate of separation of infinitesimally close trajectories. In the current study, the LLE of the preprocessed NIRS time series in different sessions were estimated using the method proposed in [22]. The LLE $\lambda_1$ is defined as $d(t) = C \cdot e^{\lambda_1 \cdot t}$, where $d(t)$ is the average divergence at time $t$ and $C$ is a constant that normalizes the initial separation.

The first step in LLE estimation is to reconstruct the attractor dynamics from a single time series. We selected the time delay $\tau$ using the C–C method introduced in [16], the embedding dimension $m$ using the G–P method from [5], and the mean period $T$ using the fast Fourier transform. For an $N$-point time series, $\{y_1, y_2, \ldots, y_N\}$, the reconstructed trajectory $\boldsymbol{X} \in R^{[N-(m-1)\tau] \times m}$ can be expressed as a matrix wherein each row is a vector $\boldsymbol{X}_i = [y_i\, y_{i+\tau} \ldots y_{i+(m-1)\tau}]$, where $i = 1, 2, \ldots, N-(m-1)\tau$.

After reconstructing the dynamics, the algorithm locates the nearest neighbor of each point on the trajectory. The nearest neighbor $\boldsymbol{X}_{i'}$ of a particular point $\boldsymbol{X}_i$ is found by searching for the point that minimizes the distance to $\boldsymbol{X}_i$. This is expressed as $d_i(0) = \min \left\| \boldsymbol{X}_i - \boldsymbol{X}_{i'} \right\|, \left| i - i' \right| > T$, where $d_i(0)$ is the initial distance from the $i$th point to its nearest neighbor, $T$ indicates the mean period, and $||\cdot||$ denotes the Euclidean norm.

From the definition of $\lambda_1$, it is assumed that the $i$th pair of the nearest neighbor diverges at the approximate rate given by the LLE: $d_i(k) \approx C_i \cdot e^{\lambda_1 \cdot (k \cdot \Delta t)}$, where $k$ indicates the time step. By taking the logarithm of both sides, $\ln d_i(k) \approx \ln C_i + \lambda_1 \cdot (k \cdot \Delta t)$ is obtained, where $k = 1, 2, \ldots, \min(N-(m-1)\tau - i, N-(m-1)\tau - i')$. The last equation represents a set of approximately parallel lines, each with a slope roughly proportional to $\lambda_1$. The LLE is easily and accurately calculated by means of a least-square fit to the "average" line. The process of averaging is critical to the accurate calculation of LLE values for small and noisy data sets [22].

After pre-processing, we categorized the time series into three sets preparatory to examine the chaotic characteristics. Set A is of the time series recorded from the channels containing the FORs during the stimulus sessions, set B is of the time series recorded (from the same channels as in Set A) during the stimulus sessions under the control condition, and set C is of those recorded during the rest sessions. In order to statistically balance the three sets, the estimated LLEs of the rest-related response were calculated over the same number of stimulus-related epochs randomly selected from the total number of rest epochs. We estimated the LLE of the time series in each session and averaged them to derive a group level result. The LLE values for the FORs and non-FORs were statistically assessed using $t$-test ($p < 0.05$).

We used the Rossler chaotic time series presented in [5] to examine the performance of the LLE-estimation algorithm. The system has an expected LLE of 0.0677. We used the time series $u$ for phase reconstruction and LLE estimation. Different lengths of the time series were selected as 500, 1000, and 3000 points, and the estimated LLEs for those were 0.0673, 0.068, and 0.676.

ICA cannot identify sequences of independent components. Therefore, we used matrix $\boldsymbol{A}$ as a tool to determine which component was related to the noises (e.g. the heart-pulse noise and measurement noise), so that they be removed from the raw signal. Fig. 2(a) shows a representative matrix $\boldsymbol{A}$ of subject 1 (wavelength 760 nm). In this matrix, each cell with index ($p$, $q$) represents the weight relating the $q$th component to the $p$th data series. The weights of components 1–5, in the bottom row, are relatively large, indicating that these components contribute to the signal measured from the collocated channel. Therefore, they need to be removed from the component matrix. Matrix $\boldsymbol{A}$ of every subject in the current study showed a similar pattern.

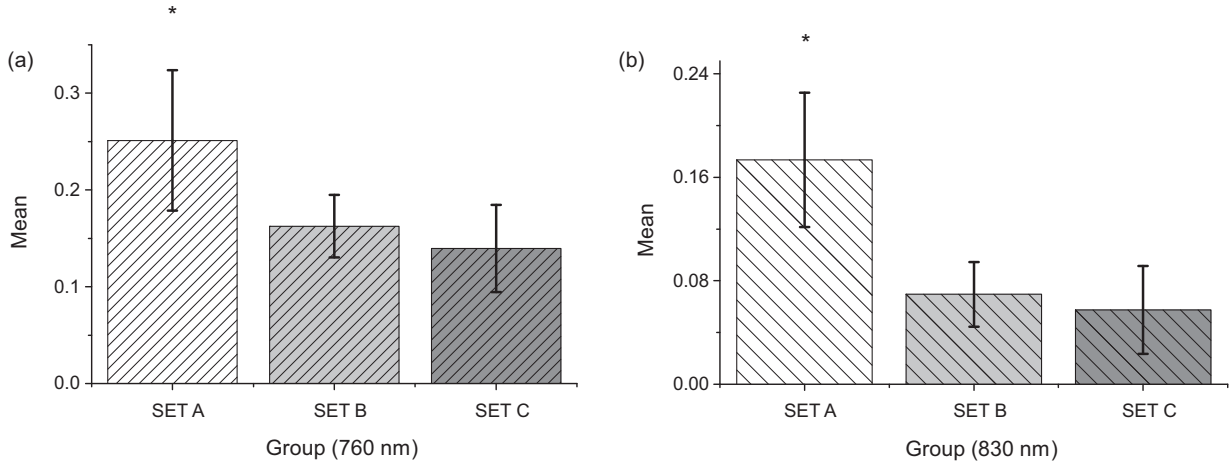


**Fig. 4.** The estimated LLEs under different conditions (the asterisk indicates a significant $t$-value, $p < 0.05$): (a) wavelength 760 nm, (b) wavelength 830 nm.

Fig. 2(b) shows the 7 s data of independent component 1 (subject 1, wavelength 760 nm). The data clearly show the heart-pulse noise separated from the raw signal, and matrix ***A*** indicates that this component contributes to most of the channels, including the collocated channel. Therefore, it was removed from the component matrix. After removing the component-related noises, the rest of the components were restored to the observed signal in each channel.

Fig. 3 shows the averaged FORs found by event-related averaging in all subjects. Panels (a) and (b) plot the averaged FORs and rest epochs at the 760 nm and 830 nm wavelengths, respectively. Panels (c) and (d) plot the averaged time series under the control condition and rest epochs at the two wavelengths. Among the ten subjects, one subject's data at 830 nm and two subjects' data at 760 nm were excluded since no significant point was found. For five subjects, the FORs were found in channel 3, whereas in the rest of the subjects, they were found in channel 4. The FORs showed a significant decrease from the base line within 300–400 ms after the tactile stimulus at both wavelengths. By contrast, the averaged signal under the control condition and in the rest sessions showed no significant decrease.

Fig. 4 shows the estimated LLEs under different conditions. The detected NIRS time series at both wavelengths were completely chaotic. However, the FOR time series recorded in the stimulus sessions were significantly more chaotic than the non-FOR time series recorded in the rest sessions. Moreover, the time series recorded under the control condition had similar chaotic level compared with the non-FOR time series.

Chaos denotes the chaotic motion generated by nonlinear systems whose dynamical laws uniquely determine the evolution of its states. The present study first confirmed that tactile-stimulus-evoked FORs can be found in the somatosensory cortex using continuous-wave NIRS equipment, and then analyzed the chaotic characteristics of the FOR time series.

FORs reflect the optical property changes of neurons as evoked by stimuli or mental tasks. Due to their outstanding temporal resolution and good spatial resolution, FORs can be considered to provide an alternative means of understanding brain function and connectivity. However, the detectability of FORs remains controversial. Previous studies have analyzed different aspects of FORs in different brain areas. Some have claimed that FORs could not be detected in NIRS time series. In the current study, however, we were able to find FORs evoked by tactile stimulus in the somatosensory cortex. Furthermore, the estimated LLEs indicated that the FOR time series were more chaotic than the non-FOR time series. The overall results strongly suggested that the LLE-evaluated chaos level can be used as an index indicating the existence of FORs over a NIRS time series and, thereby, different states of pertinent brain activity.

## Acknowledgement

This research was supported by the World Class University program through the National Research Foundation of Korea funded by the Ministry of Education, Science and Technology, Republic of Korea (grant no. R31-20004).

## References

[1] R. Barbour, H. Graber, Y. Pei, C. Schmitz, Imaging of vascular chaos, in: B. Chance, R.R. Alfano, B.J. Tromberg, M. Tamura, E.M. Sevick-Muraca (Eds.), Optical Tomography and Spectroscopy of Tissue IV. Proceedings of SPIE, vol. 4250, 2001, pp. 577–590.
[2] D.A. Boas, A.M. Dale, M.A. Franceschini, Diffuse optical imaging of brain activation: approaches to optimizing image sensitivity, resolution, and accuracy, Neuroimage 23 (2004) S275–S288.
[3] L.B. Cohen, R.D. Keynes, D. Landowne, Changes in light scattering that accompany the action potential in squid giant axons: potential-dependent components, Journal of Physiology 224 (1972) 701–725.
[4] M.A. Franceschini, D.A. Boas, Noninvasive measurement of neuronal activity with near-infrared optical imaging, Neuroimage 21 (2004) 372–386.
[5] P. Grassberger, I. Procaccia, Characterization of strange attractors, Physical Review Letters 50 (1983) 346–349.
[6] G. Gratton, P.M. Corballis, E.H. Cho, M. Fabiani, D.C. Hood, Shades of gray-matter – noninvasive optical-images of human brain responses during visual-stimulation, Psychophysiology 32 (1995) 505–509.
[7] G. Gratton, M. Fabiani, The event-related optical signal (EROS) in visual cortex: replicability, consistency, localization, and resolution, Psychophysiology 40 (2003) 561–571.
[8] G. Gratton, M. Fabiani, Shedding light on brain function: the event-related optical signal, Trends in Cognitive Sciences 5 (2001) 357–363.
[9] G. Gratton, M. Fabiani, P.M. Corballis, D.C. Hood, M.R. GoodmanWood, J. Hirsch, K. Kim, D. Friedman, E. Gratton, Fast and localized event-related optical signals (EROS) in the human occipital cortex: comparisons with the visual evoked potential and fMRI, Neuroimage 6 (1997) 168–180.
[10] G. Gratton, M. Fabiani, D. Friedman, M.A. Franceschini, S. Fantini, P. Corballis, E. Gratton, Rapid changes of optical-parameters in the human brain during a tapping task, Journal of Cognitive Neuroscience 7 (1995) 446–456.
[11] G. Gratton, M. Fabiani, M.R. Goodman-Wood, M.C. Desoto, Memory-driven processing in human medial occipital cortex: an event-related optical signal (EROS) study, Psychophysiology 35 (1998) 348–351.
[12] G. Gratton, M.R. Goodman-Wood, M. Fabiani, Comparison of neuronal and hemodynamic measures of the brain response to visual stimulation: an optical imaging study, Human Brain Mapping 13 (2001) 13–25.
[13] X.-S. Hu, K.-S. Hong, S.S. Ge, M.Y. Jeong, Kalman estimator- and general linear model-based on-line brain activation mapping by near-infrared spectroscopy, Biomedical Engineering Online 9 (2010) 82.
[14] A. Hyvarinen, E. Oja, Independent component analysis: algorithms and applications, Neural Networks 13 (2000) 411–430.
[15] H. Ichikawa, S. Kanazawa, M.K. Yamaguchi, R. Kakigi, Infant brain activity while viewing facial movement of point-light displays as measured by near-infrared spectroscopy (NIRS), Neuroscience Letters 482 (2010) 90–94.

[16] H.S. Kim, R. Eykholt, J.D. Salas, Nonlinear dynamics, delay times, and embedding windows, Physica D 127 (1999) 48–60.
[17] A.V. Meduedev, J. Kainerstorfer, S.V. Borisov, R.L. Barbour, J. VanMeter, Event-related fast optical signal in a rapid object recognition task: improving detection by the independent component analysis, Brain Research 1236 (2008) 145–158.
[18] G. Morren, M. Wolf, P. Lemmerling, U. Wolf, J.H. Choi, E. Gratton, L. De Lathauwer, S. Van Huffel, Detection of fast neuronal signals in the motor cortex from functional near infrared spectroscopy measurements using independent component analysis, Medical and Biological Engineering and Computing 42 (2004) 92–99.
[19] H. Obrig, A. Villringer, Beyond the visible – imaging the human brain with light, Journal of Cerebral Blood Flow and Metabolism 23 (2003) 1–18.
[20] S. Perrey, Non-invasive NIR spectroscopy of human brain function during exercise, Methods 45 (2008) 289–299.
[21] T. Rinne, G. Gratton, M. Fabiani, N. Cowan, E. Maclin, A. Stinard, J. Sinkkonen, K. Alho, R. Naatanen, Scalp-recorded optical signals make sound processing in the auditory cortex visible? Neuroimage 10 (1999) 620–624.
[22] M.T. Rosenstein, J.J. Collins, C.J. De Luca, A practical method for calculating largest Lyapunov exponents from small data sets, Physica D – Nonlinear Phenomena 65 (1993) 117–134.
[23] J. Steinbrink, F.C.D. Kempf, A. Villringer, H. Obrig, The fast optical signal-robust or elusive when non-invasively measured in the human adult? Neuroimage 26 (2005) 996–1008.
[24] J. Steinbrink, M. Kohl, H. Obrig, G. Curio, F. Syre, F. Thomas, H. Wabnitz, H. Rinneberg, A. Villringer, Somatosensory evoked fast optical intensity changes detected non-invasively in the adult human head, Neuroscience Letters 291 (2000) 105–108.
[25] H. Tomioka, B. Yamagata, T. Takahashi, M. Yano, A.J. Isomura, H. Kobayashi, M. Mimura, Detection of hypofrontality in drivers with Alzheimer's disease by near-infrared spectroscopy, Neuroscience Letters 451 (2009) 252–256.
[26] Q.D.K. Truong, N. Yuichi, N. Masahiro, Recognizing brain motor imagery activities by identifying chaos properties of oxy-hemoglobin dynamics time series, Chaos Solitons and Fractals 42 (2009) 422–429.